Acta Cryst. (1997). A53, 484–492

A Universal Treatment of X-ray and Neutron Diffraction in Crystals. I. Theory†

HUA-CHEN HU

China Institute of Atomic Energy, Graduate School of Nuclear Industry, PO Box 275(18), Beijing 102413, People's Republic of China. E-mail: ciaednp@sun.ihep.ac.cn

(Received 19 May 1995; accepted 13 March 1997)

Abstract

The reflection power ratio P_H/P_0, transmission power ratio P_T/P_0 and absorption power ratio P_A/P_0 for a mosaic crystal plate under asymmetric Bragg and Laue geometry are obtained by solving power transfer equations employing three dimensionless parameters: an asymmetry factor b, the ratio ξ of the absorption to the scattering cross section, and the reduced thickness A_k of the crystal. Expressions are given for the optimum monochromator thickness for asymmetric Laue geometry, and the angular dependence of P_H/P_0, P_T/P_0 for Bragg geometry in the crystals having different ξ_0 and A_{k0}. As a demonstration of the feasibility of this method, the integrated reflection power ratio experiment by Mathieson [*Acta Cryst.* (1975), **A31**, 769–774] is reanalyzed and good agreement is obtained. The standard formulae for integrated reflection by a mosaic crystal given in *International Tables for X-ray Crystallography* [(1972). Birmingham: Kynoch Press] based on the kinematic approximation are shown to be only the limiting case of the exact solution for $\xi_0 \gg 1$.

1. Introduction

The diffraction process for X-rays and neutrons in an infinite plane-parallel mosaic crystal is a basic and important problem of crystallography, and many treatments from different approaches have been given in the past several decades. The first expressions for the variation of integrated reflection intensity ratio with degree of asymmetry factor b were given for X-rays by Debye & Menke (1931). Later experiments by Gay, Hirsch & Kellar (1952) showed, however, that this equation failed to describe the strong reflections in thick crystals with small mosaic spread. Bacon & Lowde (1948) systematically investigated the diffraction process for both neutrons and X-rays for absorbing plane mosaic crystals in the Bragg and Laue cases but only in the symmetrical case. Werner & Arrott (1965), Werner, Arrott, King & Kendrick (1966) analyzed the behavior of multiple Bragg reflections as a two-dimensional problem in semi-infinite and bounded mosaic crystals, and showed that its reflection power ratio ['reflecting power' in Hu & Fang (1993)] has the value $P_H/P_0 = 1/|b|$ and 1 for $|b| > 1$ and $|b| \leq 1$, respectively, in a non-absorbing crystal. Dietrich & Als-Nielsen (1965) and Fischer (see Graf, 1983) found the mistake made by Bacon & Lowde (1948) in obtaining the solutions for reflection power ratio under asymmetical geometry and deduced the correct expressions. All these previous treatments dealt with only part of the problem and thus several important aspects of the diffraction behavior remained unclear.

We introduce here a unified theory that describes all the diffraction processes and explores several important problems that are still obscure. The present paper is the fourth in a series. The first, by Hu (1992), introduced a new method for the derivation of the reflection power ratio and transmission power ratio for deformed mosaic crystals based on a layer coupling model, which gave good agreement with published experimental data for bent Cu crystals. The second paper, by Hu, Yang & Wang (1993), applied this model to investigate the diffraction properties of a bent mosaic monochromator at different neutron wavelengths. The third paper, by Hu & Fang (1993), gave exact solutions of the power transfer equations for plane-parallel and bent mosaic crystals in asymmetric Bragg and Laue geometry for the non-absorbing case, $\mu = 0$.

In the present paper, the theory is generalized to cover the absorbing case, $\mu \neq 0$. The exact solutions for the asymmetric Bragg and Laue geometries are given in §2. §3 is a detailed physical interpretation of these results. The dependence of the reflection, transmission and absorption power ratio, particularly the integrated reflection power ratio (IRPR), on the three dimensionless parameters b, ξ and the reduced thickness A_k of the crystal are analyzed and presented through a series of graphs. The advantage of using ξ, the ratio of absorption cross section to scattering cross section, instead of using these two quantities independently is pointed out and the optimum crystal thickness in asymmetrical Laue geometry is given.

§4 is an example of an application of the present theory. The change of the IRPR with b for 200 reflection from an LiF single crystal measured by Mathieson (1975) is reanalyzed and very good agreement is obtained without use of a surface-layer effect. The following paper (Hu, 1997; hereafter referred to as II) deals with the extinction problem analyzed by use of the theory developed in this paper.

† Project supported by National Natural Science Foundation of China and Science Foundation of Nuclear Industry of China.

2. Exact solutions of the power transfer equations for asymmetric Bragg and Laue geometry in a plane mosaic crystal

The Hamilton–Darwin intensity (current density) transfer equations (here referred to as H–D equations) (see Hamilton, 1957)

$$dI_0/dx_0 = -\Sigma_t I_0 + \Sigma_s I_H \quad (1a)$$
$$dI_H/dx_H = -\Sigma_t I_H + \Sigma_s I_0 \quad (1b)$$

can be reduced to the one-dimensional power transfer equations for an infinite plane-parallel crystal plate with an asymmetry angle χ and thickness t_0 (see Hu & Fang, 1993):

$$dP_0/dt = -\Sigma_t P_0/\gamma_0 + \Sigma_s P_H/|\gamma_H| \quad (2a)$$
$$dP_H/dt = -\Sigma_t P_H/\gamma_H + \Sigma_s P_0|\gamma_H|/\gamma_0\gamma_H, \quad (2b)$$

where $\Sigma_t = \Sigma_s + \mu$, $\gamma_0 = \cos\theta_0 = \hat{\mathbf{x}}_0 \cdot \hat{\mathbf{n}}$, $\gamma_H = \cos\theta_H = \hat{\mathbf{x}}_H \cdot \hat{\mathbf{n}}$ and Σ_s is the diffraction cross section per unit volume. μ is the absorption cross section per unit volume [linear absorption coefficient for X-rays or the total attenuation coefficient for neutrons as defined by Freund (1983)].

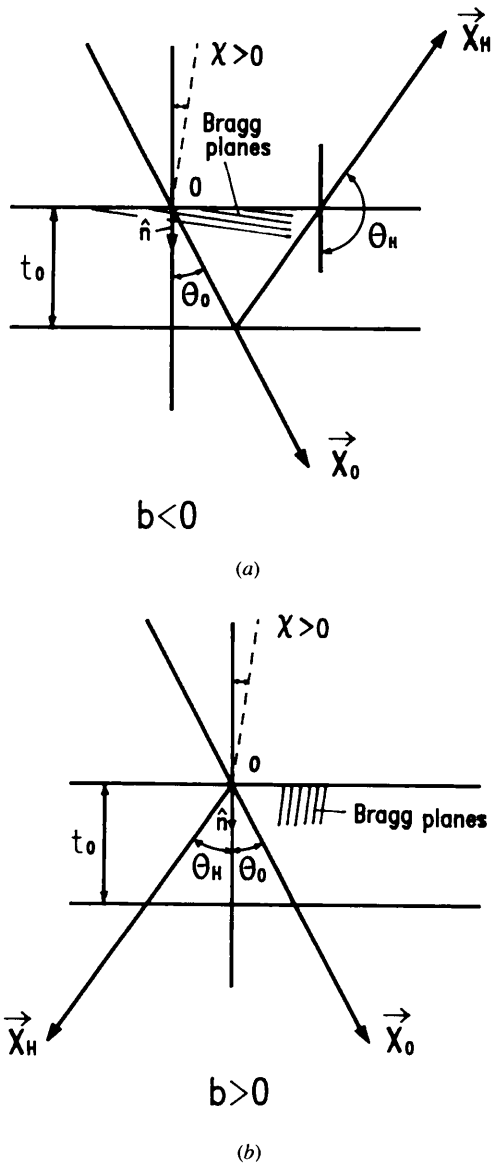

Fig. 1. Schematic diagrams of the geometry for (*a*) the Bragg case and (*b*) the Laue case.

The solutions of the power transfer equations (2*a*) and (2*b*) for Bragg and Laue geometries in a non-absorbing plane mosaic crystal were published by Hu & Fang (1993) and their notation will be used here. The schematic diagrams for the Bragg case and the Laue case are shown in Figs. 1(*a*) and (*b*), respectively.

The reflection power ratio P_H/P_0, transmission power ratio P_T/P_0 and absorption power ratio P_A/P_0 in a plane mosaic crystal with absorption for asymmetric Bragg and Laue geometries were obtained by solving these equations.

The boundary condition is

$$P_H(t_0)/P_0 = 0 \quad (3)$$

for the Bragg case and

$$P_H(0)/P_0 = 0 \quad (4)$$

for the Laue case and, from the principle of total power conservation:

$$P_H/P_0 + P_T/P_0 + P_A/P_0 = 1. \quad (5)$$

We introduce three dimensionless parameters:

(i) $b = \cos\theta_0/\cos\theta_H$, the asymmetry parameter:

$$b = -\sin(\theta_B + \chi)/\sin(\theta_B - \chi) \quad (6)$$

for the Bragg case and

$$b = \cos(\theta_B + \chi)/\cos(\theta_B - \chi) \quad (7)$$

for the Laue case;

(ii) $\xi = \mu/\Sigma_s$: the ratio of absorption cross section to the coherent elastic scattering cross section;

(iii) $A_k = \Sigma_s t_0/\cos\theta_0$: the reduced thickness of the crystal expressed in units of $\cos\theta_0/\Sigma_s$ (see Hu & Fang, 1993).

$\Sigma_s = QW(\Delta\theta_0)$ and $W(\Delta\theta_0)$ is the Gaussian distribution for the mosaic blocks at angular deviation $\Delta\theta_0$:

$$W(\Delta\theta_0) = [1/\eta(2\pi)^{1/2}]\exp\{-[\Delta\theta_0]^2/2\eta^2\}. \quad (8)$$

For non-polarized X-rays,

$$Q = \left(\frac{e}{mc^2}\right)^2 \frac{|F_H|^2 N^2 \lambda^3 p}{\sin 2\theta_B} \tag{9}$$

$$p = (1 + \cos^2 2\theta_B)/2. \tag{10}$$

With $u = [(1-b)^2(\xi+1)^2 + 4b]^{1/2}$, $v = (1-b)(\xi+1)$ and $w = (1+b)(\xi+1)$, the solutions can be expressed as follows:

(*a*) Bragg case

$$\frac{P_H}{P_0} = \frac{2[1 - \exp(-uA_k)]}{(u+v) + (u-v)\exp(-uA_k)} \tag{11}$$

for all b and ξ except $\xi = 0$, $b = -1$. For the symmetric Bragg case ($b = -1$), (11) becomes

$$P_H/P_0 = \{1 - \exp[-2(\xi^2 + 2\xi)^{1/2}A_k]\}\{(\xi^2 + 2\xi)^{1/2} + \xi + 1 + [(\xi^2 + 2\xi)^{1/2} - (\xi + 1)] \times \exp[-2(\xi^2 + 2\xi)^{1/2}A_k]\}^{-1} \tag{12}$$

$$P_H/P_0 = A_k/(1 + A_k) \tag{13}$$

for $\mu = 0$, $b = -1$.

$$\frac{P_T}{P_0} = \frac{2u\exp[-(w+u)A_k/2]}{(u+v) + (u-v)\exp(-uA_k)} \tag{14}$$

$$P_A/P_0 = \{(u + v - 2) - 2u\exp[-(w+u)A_k/2] + (u - v + 2)\exp(-uA_k)\} \times [(u+v) + (u-v)\exp(-uA_k)]^{-1}. \tag{15}$$

(*b*) Laue case

$$P_H/P_0 = \{\exp[-(w-u)A_k/2] - \exp[-(w+u)A_k/2]\}/u. \tag{16}$$

For the symmetric Laue case ($b = 1$), (16) becomes

$$P_H/P_0 = \exp[-\xi A_k][1 - \exp(-2A_k)]/2 \tag{17}$$

$$P_T/P_0 = \{(u+v)\exp[-(w+u)A_k/2] + (u-v)\exp[-(w-u)A_k/2]\}/2u \tag{18}$$

$$P_A/P_0 = 1 - \{[1 + (u-v)/2]\exp[-(w-u)A_k/2] - [1 - (u+v)/2]\exp[-(w+u)A_k/2]\}/u. \tag{19}$$

The same P_H/P_0 can be derived from either the two-dimensional solution of the H–D equations (1*a*) and (1*b*) (Zhou, Yang & Hu, 1995) as shown in Appendix *A* or the numerical calculation from the layer coupling model (Hu, 1992). All these confirm the consistency of these theories.

Values of the reflection intensity ratio I_H/I_0 and transmission intensity ratio I_T/I_0 for a collimated monoenergetic incident beam of X-rays (or neutrons) of infinite extension may be defined through the relationships

$$I_H/I_0 = |b|P_H/P_0 \tag{20}$$

and

$$I_T/I_0 = P_T/P_0. \tag{21}$$

One should note that P_H/P_0 can be used either in the case of an incident beam of limited width or a beam of infinite extension, while the I_H/I_0 is valid only for the latter case.

Expressions (3)–(21) are general formulae valid for both symmetric and asymmetric Bragg and Laue geome-

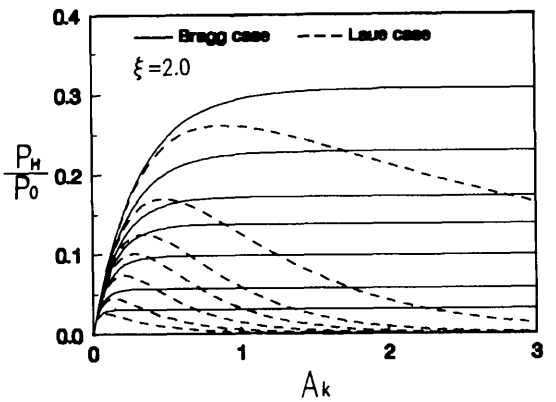

Fig. 2. Dependence of the reflection power ratio P_H/P_0 on the reduced thickness A_k of a mosaic plane crystal for the Bragg case and the Laue case. The values of the parameter $|b|$ for the curves from top to bottom are: 0.1, 0.5, 1.0, 1.5, 2.5, 5.0, 10.0. The corresponding curves for $\xi = 0$ were given by Hu & Fang (1993).

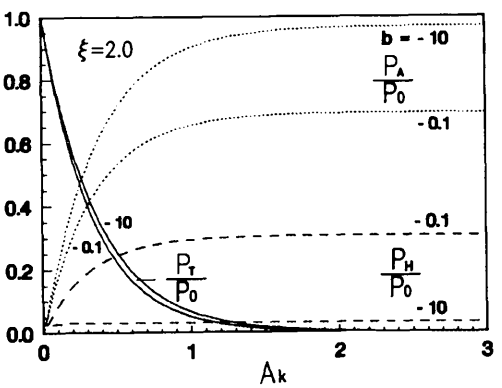

Fig. 3. Dependence of reflection power ratio P_H/P_0 (dashed curve), transmission power ratio P_T/P_0 (continuous curve) and absorption power ratio P_A/P_0 (dotted curve) on the reduced thickness A_k for $\xi = 2$ in the Bragg case.

tries, with and without absorption, for X-ray, neutron or electron diffraction in a plane mosaic crystal. Dietrich & Als-Nielsen (1965) and Fischer (see Graf, 1983) have obtained similar expressions to (16) and (11) but their formalism is complex and it is difficult to understand the physical meaning of their formulae. Thus, their application is limited.

3. Physical interpretation of the solutions

3.1. *The effect of asymmetric geometry and absorption*

From the solution of the power transfer equation, we can see the comprehensive and complicated dependence of the reflection power ratio, transmission power ratio *etc.* on the asymmetry parameter b, the ratio of absorption cross section to scattering cross section ξ and the reduced thickness A_k, as illustrated in Figs. 2–5.

For both symmetric and asymmetric geometry, one can see from Fig. 2 that: (i) for the same ξ and A_k, P_H/P_0 decreases with increasing $|b|$; (ii) for the same ξ and b, in the Bragg case P_H/P_0 increases with A_k when A_k is small, and saturates as A_k increases, while in the Laue case with absorption, P_H/P_0 goes through a maximum value at a certain $A_k^{\max}$, whose expression is given below. For the same A_k, P_H/P_0 increases with increasing $1/\xi$, and most strongly as $\xi \to 0$ (Hu & Fang, 1993). For the symmetric geometry and without absorption, the maximum reflection power ratio attainable in the Laue case is only 0.5, half of the maximum reflecting power ratio attainable in the Bragg case; but this ratio can exceed 0.5 as ξ increases, and the reflection power ratio is larger than 0.5 for the Laue case with $\mu \simeq 0$ and $b < 1$.

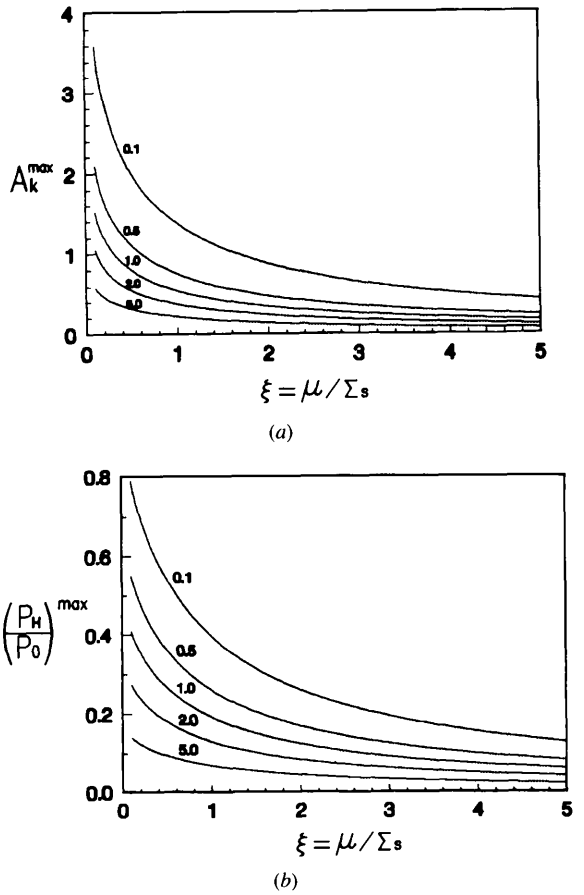

Fig. 4. (*a*) The dependence of $A_k^{\max}$ on ξ. (*b*) The dependence of $(P_H/P_0)^{\max}$ on ξ in the Laue case. The parameters on the curves are b.

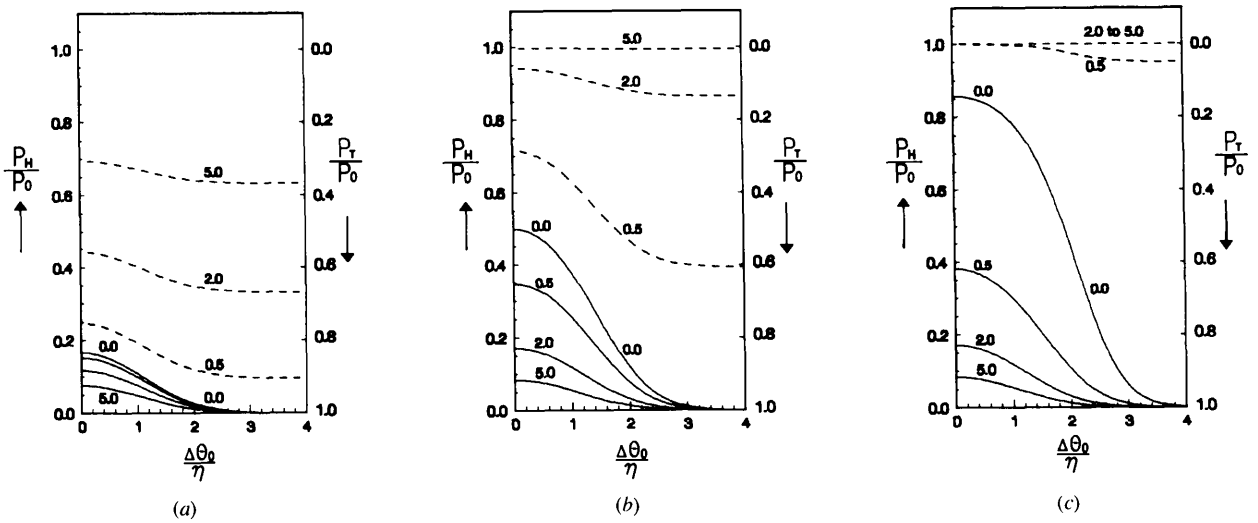

Fig. 5. Rocking curves of the reflection power ratio (continuous curves) and transmission power ratio (dashed curves) in the symmetric Bragg case for different values of ξ_0 given on the curves. (*a*) $A_{k0} = 0.2$; (*b*) $A_{k0} = 1.0$; (*c*) $A_{k0} = 6.0$. Note that the rocking curves for P_H/P_0 and P_T/P_0 are identical when $\xi_0 = 0$.

For a crystal with a given value of ξ, the value of P_H/P_0 in the Bragg case decreases with $|b|$, while P_A/P_0 increases with $|b|$, as shown in Fig. 3. This is because, for the same path length traveled by the incident beam, the diffracted beam for smaller $|b|$ comes from a position closer to the crystal surface than for larger $|b|$, so the diffracted beam experiences less absorption and the resultant reflection power ratio is larger.

3.2. A_k^{max} *for asymmetric Laue geometry*

$A_k^{\max}$ is defined as the value of A_k when P_H/P_0 is a maximum. Its value for asymmetric Laue geometry can be obtained through the relationship

$$\mathrm{d}(P_H/P_0)/\mathrm{d}A_k = 0, \tag{22}$$

which gives the expression

$$A_k^{\max} = \frac{1}{u}\ln\frac{(1+b)(\xi+1)+u}{(1+b)(\xi+1)-u}. \tag{23}$$

Figs. 4(*a*) and (*b*) depict the dependence of $A_k^{\max}$ and $(P_H/P_0)^{\max}$, respectively, on ξ for an absorbing crystal with different b values for the Laue case.

3.3. *Rocking curves*

Some important conclusions follow from the calculated rocking curves of the reflection power ratio and transmission power ratio. With the assumption of a Gaussian distribution of the mosaic blocks, Figs. 5(*a*)–(*c*) depict the angular dependence of P_H/P_0 and P_T/P_0 for the reduced thickness of the crystal, $A_{k0} = 0.2$, 1 and 6. P_A/P_0 is not shown since it can be obtained by the principle of total power conservation when P_H/P_0 and P_T/P_0 are known. The values of Σ_s, ξ and A_k at $\Delta\theta_0 = 0$ are defined as

$$\Sigma_{s0} = Q/(2\pi)^{1/2}\eta \tag{24}$$

$$\xi_0 = \mu/\Sigma_{s0} \tag{25}$$

$$A_{k0} = \Sigma_{s0}t_0/\cos\theta_0 = Qt_0/(2\pi)^{1/2}\eta\cos\theta_0 \tag{26}$$

and the expression

$$\mu t_0/\cos\theta_0 = \xi_0 A_{k0} \tag{27}$$

can be obtained by relating these parameters.

One can see from Figs. 5(*a*)–(*c*) that:

(i) For the same ξ_0, the FWHM of P_H/P_0 increases with increasing A_{k0};

(ii) The shape of rocking curves for P_H/P_0 remains the same for $\xi_0 \geq 5$ and $A_{k0} \geq 0.4$, where the IRPR saturates (see Fig. 6*a*) and $P_T/P_0 \simeq 0$ for all $\Delta\theta_0$;

(iii) For a thick crystal, in the transition region between non-absorption and absorption, *i.e.* from $\xi_0 = 0$ to $\xi_0 > 0$, the FWHM for P_H/P_0 decreases with increasing ξ_0; and, when $\xi_0 > 10$, it approaches the 'secondary-extinction-free' limiting value, $2(2\ln 2)^{1/2}\eta = 2.355\eta$, the true mosaic spread (see Fig. 4 of II). We note that, in the normal case of X-ray diffraction, the condition $\xi_0 > 10$ is generally met and the shape of the rocking curve nearly represents the true mosaic distribution. But for neutron diffraction this condition usually does not hold, since in most cases $\mu/\Sigma_{s0} \simeq 0$; and from Fig. 7 one can see that the FWHM for the rocking curve will be several times the true mosaic spread;

(iv) Fig. 5(*a*) shows that P_A/P_0 becomes almost independent of rocking angle when $A_{k0} \leq 0.2$; the value of P_T/P_0 at the tail of the rocking curve is $\exp(-\mu t_0/\cos\theta_0)$ in the limiting case when $\Sigma_s \to 0$, *i.e.* $\xi \to \infty$.

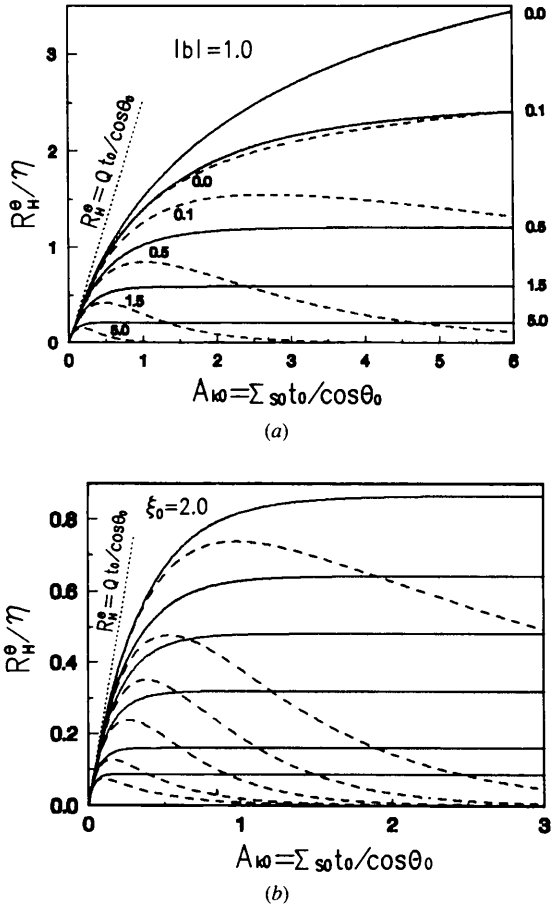

Fig. 6. R_H^θ/η for a plane mosaic crystal as a function of the reduced thickness A_{k0}. Bragg case (continuous curve); Laue case (dashed curve). (*a*) The parameters given on the curves are ξ_0; (*b*) the parameter $|b|$ for the curves from top to bottom are 0.1, 0.5, 1, 2, 5, 10.

3.4. *Integrated reflection power ratio*

The IRPR R_H^θ is defined by the expression

$$R_H^\theta(\xi_0, A_{k0}, b)/\eta = \int_{-\infty}^{+\infty} (P_H/P_0)\left(\xi(\Delta\theta_0/\eta), A_k(\Delta\theta_0/\eta), b\right) \mathrm{d}(\Delta\theta_0/\eta). \quad (28)$$

The IRPR for Bragg and Laue geometries can be obtained by substituting (11)–(13) and (16)–(17) into (28). When ξ is very large (*i.e.* $\mu \gg \Sigma_s$), for the Bragg case (11) becomes

$$P_H/P_0 = \{1 - \exp[-(1-b)\mu t_0 \sec\theta_0]\} \times [(1-b)(\xi+1)]^{-1} \quad (29)$$

and substituting $\xi = \mu/\Sigma_s$ into (29) with $\xi \gg 1$, we obtain

$$R_H^\theta = Q\{1 - \exp[-(1-b)\mu t_0 \sec\theta_0]\}/[(1-b)\mu]. \quad (30)$$

The corresponding expressions for the Laue geometry for $b \neq 1$ are

$$P_H/P_0 = \{\exp[-b(\xi+1)A_k] - \exp[-(\xi+1)A_k]\} \times [(1-b)(\xi+1)]^{-1}, \quad (31)$$

$$R_H^\theta = [Q/(1-b)\mu][\exp(-\mu t_0 \sec\theta_H) - \exp(-\mu t_0 \sec\theta_0)] \quad (32)$$

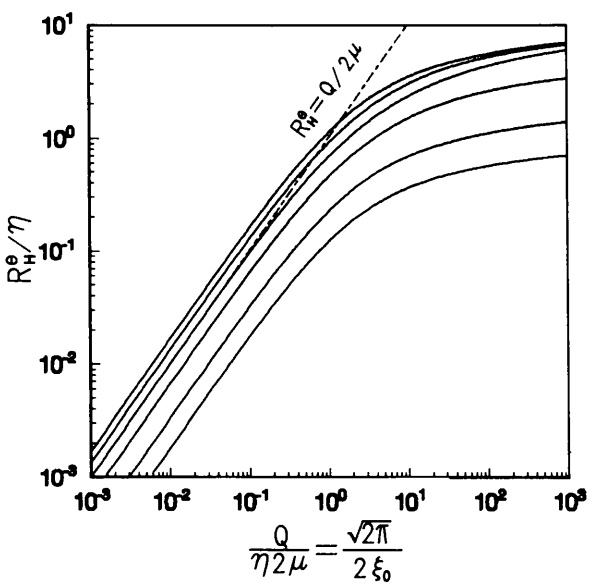

Fig. 7. The relationship between $Q/2\mu$ and R_H^θ from a plane mosaic crystal of infinite thickness in the Bragg case for $b = -0.2, -0.5, -1, -2, -5, -10$ for the curves from top to bottom.

for $b = 1$, substituting $\xi = \mu/\Sigma_s$ into (17) with $\xi \gg 1$, we obtain

$$R_H^\theta = Qt_0 \sec\theta_B \exp(-\mu t_0 \sec\theta_B). \quad (33)$$

Equations (30), (32) and (33) are identical with the kinematic formulae for integrated reflection QA_c published in *International Tables for X-ray Crystallography* (1972) (here referred to as *ITXCr*) for a crystal with absorption. Note that for the Bragg case the sign of angle χ in the present paper is the same as that in *ITXCr* (1972), but for the Laue case it is reversed.

Fig. 6(*a*) depicts the the relationship between R_H^θ/η and A_{k0} for different ξ_0 in the symmetric geometry. If we follow the definition given by Bacon & Lowde (1948) that a thin crystal should have its IRPR within 5% of the $Qt_0/\cos\theta_0$ value, then the thickness of the thin crystal t_0 will decrease with increasing ξ_0. It can also be seen from Fig. 6(*b*) that this thickness is reduced with increasing $|b|$. When $\xi_0 = 2$, this expression is valid only in the region $A_{k0} < 0.04$ for $|b| < 1$ and $A_{k0} = 0.04/|1+b|$ for $|b| > 2$. From Figs. 6(*a*)–(*b*), we can also see that, when the thickness increases, in the Laue case the IRPR goes to a maximum, while in the Bragg case it approaches a saturation value. For a thick crystal, the saturation value of A_{k0} decreases with increasing ξ_0 or $|b|$.

Fig. 7 summarizes the relationship between R_H^θ and $Q/\eta 2\mu$ for an infinitely thick crystal with different $|b|$ in the Bragg case. At the left side, *e.g.* around $Q/\eta 2\mu = 0.1$ or $\xi_0 > 12.6$, the absorption mean free path (MFP) is much smaller than the scattering MFP. The dependence of R_H^θ on $Q/2\mu$ for different $|b|$ is demonstrated by the parallel lines in the double logarithmic plot of Fig. 7, with slope unity. Here the secondary extinction is weak and approaches zero on the extreme left as an asymptote to the dot-dashed line representing the secondary-extinction-free case. On the right side of Fig. 7, where $Q/\eta 2\mu > 10$ or $\xi_0 < 0.13$, corresponding to the larger ratio of the absorption MFP to scattering MFP, the secondary extinction increases with decreasing ξ_0, *e.g.* when $\xi_0 = 0.1$ or $Q/\eta 2\mu = 12.53$, we have $R_H^\theta/\eta = 3.82$ and 2.53 for $b = -0.1$ and $b = -1$, respectively, their ratio being 1.5. As ξ_0 further decreases, the curves move outward to the nearly non-absorbing limit ($\xi_0 = 5 \times 10^{-19}$), $R_H^\theta/\eta = 18$ for $|b| \leq 1$ and $R_H^\theta/\eta = 18/|b|$ for $|b| > 1$. The secondary-extinction factor implicit in this figure will be expressed explicitly in Fig. 4 of II.

It should be noted that all the work described above is based on the concept of reflection power ratio P_H/P_0 rather than reflection intensity ratio I_H/I_0 defined in (20). When one draws the set of curves for I_H/I_0 *versus* A_k, one sees that, in contrast with the relationship between P_H/P_0 and $|b|$ for a definite ξ and A_k, the I_H/I_0 values for large $|b|$ will be larger than those for smaller $|b|$. This is the same for the relationship between the

integrated-reflection-intensity ratio and A_{k0}. Since (2*a*) and (2*b*) given by Hu & Fang (1993) are based on a one-dimensional approximation of H–D equations for an infinite plane parallel crystal, *i.e.* by assuming that the incident radiation has an infinite extension along the crystal surface, hence the reflection intensity ratio I_H/I_0 obtained through (20) can only be applied for a very broad incident beam in both the Bragg and Laue cases. Here we shall investigate the Bragg case in more detail.

(i) When $0 < \xi_0 < 1$, as is the case for most neutron diffraction and for X-rays when μ is smaller than Σ_{s0}, the beam penetration is deep, the lateral extension of the diffracted beam is large and usually we cannot use the value of I_H/I_0 obtained from (20). We consider neutron diffraction of Cu(200) with $\eta = 10'$, $\mu = 0.42\,\text{cm}^{-1}$ for $\lambda = 1.3$ Å, $\chi = 0°$ as an example. Here, $\theta_B = 21.08°$, $Q = 47.8'\,\text{cm}^{-1}$, $\Sigma_{s0} = Q/(2\pi)^{1/2}\eta = 1.9\,\text{cm}^{-1}$, $\xi_0 = 0.22$ and the IRPR will saturate when $A_{k0} > 6$ or $t_0 > 1.1$ cm. For a pencil incident beam according to Werner, Arrott, King & Kendrick (1966), about 92% of the neutrons of the exit beam are distributed over a width of $2t_0 \cos\theta_B$ (*i.e.* 2 cm), hence the infinite-beam-width approximation is satisfied only when the width of the incident neutron beam exceeds this value by about a factor of four (*i.e.* 8 cm). However, this requirement has often been overlooked. The correct expression for the reflection-intensity ratio from an incident beam of finite width is the result derived only by using the two-dimensional H–D equations given by Werner, Arrott, King & Kendrick (1966); while, for a δ-function beam incident on a crystal of infinite thickness, the solution (36) is shown in Appendix *A*.

(ii) When $\xi_0 > 2$, the normal X-ray case, the beam penetration is shallow, usually less than half a scattering MFP, and the condition of mirror surface reflection is usually met, so that a beam width of several millimeters can already be considered as infinitely broad. The Fankuchen (1937) effect, *i.e.* the space condensation of the diffracted current density with increasing $|b|$, appears; however, it may not be as strong as in the perfect-crystal case owing to the strong absorption, and the value of I_H/I_0 is usually less than 1 because of its relatively small reflection power ratio compared with the weakly absorbing perfect crystal.

The solution for P_H/P_0, *i.e.* (11)–(13), (16) and (17), differs from the reflection intensity ratio and transmission intensity ratio given by (20) and (21), for which the incident-beam width has to be considered and the corresponding R_H^θ is independent of the incident-beam width and relates only to the ratio of incident and reflected total power. This has already been proved by use of the layer-coupling-model treatment (Hu, 1992). In an experiment, this means that a wide open detector should be used to collect all the diffracted beam.

One should note that, although in (20) $I_H/I_0 = P_H/P_0$ when $|b| = 1$, $I_H/I_0 + I_T/I_0$ will not be unity when $\mu = 0$ unless the width of the incident beam is infinite.

4. Application of the theory: reanalysis of the experiment of integrated reflection power ratio of LiF under asymmetric geometry

In this section, Mathieson's (1975) experiment is reanalyzed as a demonstration of the capabilities of the theory. For a long time, the formula in *ITXCr* (1972) corresponding to (30) was considered as describing adequately the IRPR for an absorbing mosaic crystal under asymmetric Bragg geometry. However, the integrated reflection intensity ratio measurement carried out on various crystals such as calcite, quartz, fluorite and lithium fluoride showed noticeable deviations from the theoretical prediction (Evans, Hirsch & Kellar, 1948; Gay, Hirsch & Kellar, 1952). These authors attributed this discrepancy to the existence of a layer of irregularities on the crystal surface that may cause absorption of X-rays without much contribution to reflection. The deviation remains however for a crystal with etched surface.

Mathieson (1975) measured precisely the (200) IRPR under asymmetric Bragg geometry for several different b values for an LiF single crystal having NaCl structure ($a = 4.026$ Å) with Cu $K\alpha$ X-radiation ($\lambda = 1.54$ Å). The experimental data depicted in Fig. 8 show very large deviations from the theoretical result predicted by (30), which is depicted as curve (*a*). Mathieson, like previous authors, explained the discrepancy by the surface-layer effect.

We shall reanalyze these experimental data with our method. Expression (30) based on the kinematic approximation corresponds to the extreme case when $\mu \gg \Sigma_{s0}$ in our multiple reflection treatment, depicted on the left side in Fig. 7 or curve (*a*) in Fig. 8. The other extreme

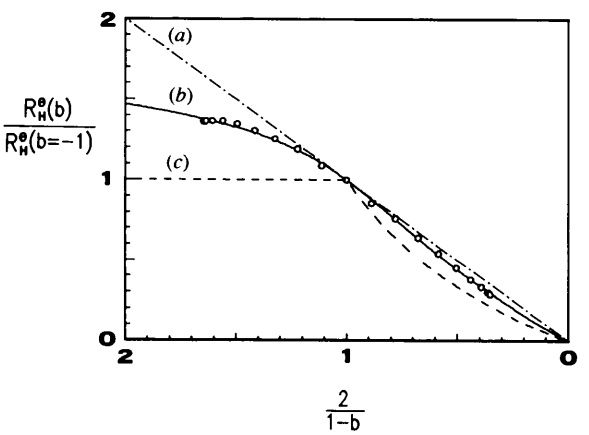

Fig. 8. Comparison of the theoretical prediction with the experimental asymmetric IRPR curve for X-rays by an LiF plane mosaic crystal: (*a*) theoretical prediction for large ξ_0; (*b*) the open circles show the experiment results obtained by Mathieson (1975) and the full curve our theoretical prediction for $\xi_0 = 0.045$; (*c*) theoretical prediction for $\xi_0 = 0$. Since $b = -\sin(\theta_B + \setminus)/\sin(\theta_B - \setminus)$, the abscissa in this figure is the same as in Fig. 5 in Mathieson (1975).

case, *i.e.* $\mu = 0$ or $\xi_0 = 0$, which corresponds to the extrapolated right side of Fig. 7 and $R_H^\theta(b)/R_H^\theta(b=-1)$, will give the values 1 and $1/|b|$ for $|b| \leq 1$ and $|b| > 1$, respectively, as depicted by curve (*c*) in Fig. 8. Neither of these extremes fits the experimental data. Lithium fluoride is composed of atoms of low atomic number Z and the crystal has a small mosaic spread, so that its 200 reflection is a strong peak with large Q value; by our definition, this corresponds to the case of $\xi_0 \simeq 0$ and in our diagram lies close to the right side in Fig. 7. This means we might expect the experimental data to lie somewhere between curves (*a*) and (*c*) in Fig. 8.

The theoretical fitting curve corresponding to these experimental conditions can be calculated from (11) and (28) by using ξ_0 as a fitting parameter. The best fit, corresponding to $\xi_0 = 0.045$, was used further to calculate η with the known parameters of the LiF 200 reflection, $\mu = 27.7\,\text{cm}^{-1}$ (Ice & Specht, 1992), $\theta_B = 22.52°$, $Q = 206'\,\text{cm}^{-1}$ and Debye–Waller factor $B_{\text{Li}} = 0.90$, $B_{\text{F}} = 0.63\,\text{Å}^2$ (Killean, Lawrence & Sharma, 1972). The final result, depicted as curve (*b*) in Fig. 8, agrees well with experiment, and the value of $\eta = 8.03''$, evaluated from ξ_0, is the only adjustable parameter. This η value corresponds to a mosaic spread of $18.9''$, which is about four times the Darwin width, $4.67''$, for the 200 reflection. From equation (2) in II, the secondary-extinction factor for the 200 reflection in symmetric geometry is $Y_\mu = 0.12$. This low value is in reasonably good agreement with the experimental value, $Y_\mu = 0.20$, obtained by Lawrence (1972) for the same reflection of LiF.

The method introduced by Kawamura & Kato (1983) is also used for fitting Mathieson's experiment by plotting the dependence of the ratio of P_H/P_0 at different b and P_H/P_0 at $b = -1$ on $2/(1-b)$. A good fit can also be obtained by a fitting parameter $\xi = 0.110$. Since $\xi = \mu/\Sigma_s$ (here Σ_s is equivalent to the coupling constant σ in Kawamura & Kato's formalism), we have $\sigma = 252\,\text{cm}^{-1}$ for the known μ value of LiF. Because the extinction distance for the LiF 200 reflection is $\Lambda = 5.68 \times 10^{-6}$ m, the correlation length of the phase factor $\tau_2 = \sigma\Lambda^2/2 = 4.04 \times 10^{-7}$ m can also be evaluated, and this gives the fitting parameter η_{KK} of the coherent blocks, namely $\eta_{KK} = 13.7''$, which is about 1.7 times the value obtained by our previous method. The value $\tau_2/\Lambda = 0.0713 \ll 1$ obtained from this fit implies that the power transfer equations are certainly valid in this case, *i.e.* the secondary extinction is predominant. If the experiment is carried out for the same sample under two different wavelengths, then the mean size of the blocks $\bar{l}$ can also be obtained by Kawamura & Kato's method.

In the analysis of his LiF data, Mathieson (1975) assumed that a layer of thickness $t_{\text{sur}} = 1.4 \times 10^{-5}$ m of absorbing but non-reflecting material on the surface of the abraded crystal is responsible for the deviation of his result from theory. However, this is questionable.

(i) If we allow Mathieson's argument and assume that the relationship represented by curve (*a*) in Fig. 8 still holds for his case without a surface layer, then μ/Σ_{s0} should be no less than 4 from Fig. 7, and the η value of the crystal would be $\eta > 15.0'$. This value is too large and highly improbable for a typical LiF crystal.

(ii) Note that the condition in which curve (*a*) in Fig. 8 is valid for the LiF case also implies that the IRPR expressed through (30) must come from the integration of P_H/P_0 expressed by (29). In such a case, the peak value of P_H/P_0 for $b = -1$ is $\Sigma_{s0}/2\mu = Q/2(2\pi)^{1/2}\eta\mu$, and for any $\eta < 1.48'$ this value will exceed unity, which is impossible. This means that the mosaic spread of the sample will be no less than $1.48'$, again a value too large for LiF.

(iii) According to Dorner (1971), the scattering from the surface layer cannot be negligible and the treatment by Mathieson (1975) is oversimplified.

For a crystal with a surface layer, the layer-coupling model (Hu, 1992) is a good choice for the evaluation of its IRPR. However, since the path length of the beam within each layer increases with the asymmetric parameter β [$\beta = (b+1)/(b-1)$], it is important to have a large enough number of layers for obtaining the exact extinction value when $|\beta|$ increases. Besides, because of the many parameters such as surface-layer thickness t_{sur}, η, η_{sur} *etc.* involved, a proper fit may require an experiment to be carried out using more than three wavelengths, and the fitting process will be quite tedious. Thus, the best way is to use a properly treated surface-layer-free crystal for such an experiment.

From all the above arguments and the good fit of the curve of Fig. 8(*b*) in this work, it is highly probable that the deviation of the experimental curve (*b*) from (*a*) is due to multiple reflection and not a surface effect.

The rather small value of $\eta = 8.03''$ obtained from our analysis of Mathieson's experiment may imply the existence of weak primary extinction. However, so far as the H–D equations treatment is still valid (Werner, 1974; Becker, 1977), one can use $Y_p\Sigma_{s0}$ instead of Σ_{s0} in power transfer equations to evaluate the same fitting curve (*b*). The only difference here is that η/Y_p will appear instead of η.

5. Conclusions

By introducing three dimensionless parameters, a very general set of solutions describing the diffraction behavior of X-rays, neutrons and electrons in mosaic crystal plates is established. It can be applied to describe crystal samples with all possible thicknesses, mosaic spreads and degrees of absorption for all types of diffraction symmetry and to evaluate the reflection power ratio, transmission power ratio, absorption power ratio and their integrated values. It is shown that the standard formulae in *ITXCr* (1972) for the integrated reflection,

i.e. (30), (32) and (33) in this paper, for a mosaic crystal are simply limiting cases of the exact solutions.

The increase of IRPR with increasing $1/|b|$, $1/\xi_0$ and A_{k0} is found to be fast and the influence of $|b|$ on R_H^θ is remarkable. All these results follow from the one-dimensional H–D equations but one can see that both the penetration depth and the lateral spread of the incident beam can be evaluated under Bragg geometry from the saturated value of A_{k0} when b and ξ_0 are defined.

The theory serves not only as a basis for the crystal extinction treatment to be described in II but may also be expected to find wide application in monochromator design under either symmetric or asymmetric geometry for X-ray, neutron and electron beams.

The reciprocity relation (see Wilkins, 1981) between the positive and negative asymmetric cases can be derived from (36), which means that the extinction factors Y_ν and Y_μ will be the same for b and $1/b$.

The author is grateful to Professor S. A. Werner of the University of Missouri, USA, and Professor T. M. Sabine of the Lucas Heights Research Laboratory, Australia, for valuable advice. The author is also grateful to Professor E. Fawcett of the University of Toronto, Canada, and Proessor. Z. Yang of the Neutron Scattering Laboratory of CIAE, China, for help and suggestions about presentation.

APPENDIX *A*
The derivation of P_H/P_0 from the two-dimensional solution of the H–D equations (1*a*) and (1*b*) (Zhou, Yang & Hu, 1995)

Assume a δ-function beam with power P_0 incident on a plane mosaic crystal of infinite thickness at the origin O for the Bragg case [Fig. 1(*a*); note that both the coordinates x_0 and x_H originate at O]. The boundary conditions are:
along the incident beam:

$$I_H(x_0, 0) = P_0 \Sigma_s^2 \exp(-\Sigma_t x_0) x_0 / \sin 2\theta_B; \qquad (34)$$

along the crystal surface from the origin O:

$$I_0(x_0, -bx_0) = 0. \qquad (35)$$

The distribution of the reflection intensity along the crystal surface will be

$$\begin{aligned} I_H(x_0, -bx_0) = (P_0 \Sigma_s / \sin 2\theta_B) \{ & I_0[2\Sigma_s(-b)^{1/2} x_0] \\ & - I_2[2\Sigma_s(-b)^{1/2} x_0] \} \\ & \times \exp[-\Sigma_t(1-b)x_0]. \end{aligned} \qquad (36)$$

The total reflection power P_H can be obtained by the integration

$$P_H = \int_0^\infty I_H(x_0, -bx_0) \sin 2\theta_B \, dx_0, \qquad (37)$$

which gives the same P_H/P_0 formula as (11) for $A_k = \infty$.

References

Bacon, G. E. & Lowde, R. D. (1948). *Acta Cryst.* **1**, 303–314.
Becker, P. J. (1977). *Acta Cryst.* A**33**, 243–249.
Debye, P. & Menke, H. (1931). *Ergeb. Tech. Rontgenkd.* **2**, 1.
Dietrich, O. W. & Als-Neilsen, J. (1965). *Acta Cryst.* **18**, 184–188.
Dorner, B. (1971). *J. Appl. Cryst.* **4**, 185–190.
Evans, R. C., Hirsch, P. B. & Kellar, J. N. (1948). *Acta Cryst.* **1**, 124–129.
Fankuchen, I. (1937). *Nature (London)*, **139**, 193–194.
Freund, A. K. (1983). *Nucl. Instrum. Methods*, **213**, 495–501.
Gay, P., Hirsch, P. B. & Kellar, J. N. (1952). *Acta Cryst.* **5**, 7–11.
Graf, H. (1983). Report HMI-B403, pp. 1–155. Hahn–Meitner Institut, Berlin, Germany.
Hamilton, W. C. (1957). *Acta Cryst.* **10**, 629–634.
Hu, H.-C. (1992). *J. Appl. Cryst.* **25**, 731–736.
Hu, H.-C. (1997). *Acta Cryst.* A**53**, 493–504.
Hu, H.-C. & Fang, Y. (1993). *J. Appl. Cryst.* **26**, 251–257.
Hu, H.-C., Yang, B. & Wang, J. (1993). *Nucl. Instrum. Methods*, A**335**, 239–242.
Ice, G. E. & Specht, E. D. (1992). *J. Appl. Cryst.* **25**, 488–494.
International Tables for X-ray Crystallography. (1972). Vol. II, p. 291. Birmingham: Kynoch Press.
Kawamura, T. & Kato, N. (1983). *Acta Cryst.* A**39**, 305–310.
Killean, R. C., Lawrence, J. L. & Sharma, V. C. (1972). *Acta Cryst.* A**28**, 405–407.
Lawrence, J. L. (1972). *Acta Cryst.* A**28**, 400–404.
Mathieson, A. McL. (1975). *Acta Cryst.* A**31**, 769–774.
Werner, S. A. (1974). *J. Appl. Phys.* **45**, 3246–3254.
Werner, S. A. & Arrott, A. (1965). *Phys. Rev.* **140**, A675–A686.
Werner, S. A., Arrott, A., King, J. S. & Kendrick, H. (1966). *J. Appl. Phys.* **37**, 2343–2350.
Wilkins, S. W. (1981). *Proc. Philos. Trans.* **299**, 275–317.
Zhou, Y.-Z., Yang, Z. & Hu, H.-C. (1995). *Acta Phys. Sin.* **44**, 726–733.